Synsint Research Group

Available online at www.synsint.com

Synthesis and Sintering

ISSN 2564-0186 (Print), **ISSN** 2564-0194 (Online)

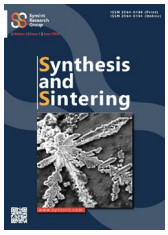

Reseach article

Microstructural transformation and recovery of rare earth elements during hydrochloric acid leaching of apatite concentrate

Erfan Mohammadzadeh *, Sayed Khatiboleslam Sadrnezhaad, Hossein Yoozbashizadeh, Mahdi Maarefvand

Department of Materials Science and Engineering, Sharif University of Technology, Azadi Ave, Tehran, P.O. Box 11155-9466, Iran

ABSTRACT

Hydrochloric acid concentration plays a pivotal role in governing the dissolution behavior of apatite and the recovery of rare earth elements (REEs) during hydrometallurgical processing. In this study, the influence of hydrochloric acid concentration on the leaching of cerium (Ce), lanthanum (La), and neodymium (Nd) from an apatite concentrate derived from iron ore processing waste was comprehensively investigated by correlating microstructural evolution with leaching performance. Response surface methodology (RSM) coupled with central composite design (CCD) was employed to evaluate the combined effects of hydrochloric acid concentration and leaching temperature on the recovery of cerium, lanthanum, and neodymium. Throughout the optimization study, the solid-to-liquid ratio (1:9) and leaching time (60 min) were maintained constant to isolate the influence of the selected variables and improve the reliability of the statistical model. Under the optimum conditions of 37 wt% HCl, a solid-to-liquid ratio of 1:9, a leaching time of 60 min, and a temperature of 65 °C, the recoveries of Ce, La, and Nd reached 94.19%, 86.33%, and 76.34%, respectively. SEM analysis of the leaching residues revealed a progressive transition from relatively smooth, well-preserved crystalline particles at low acid concentrations to severely corroded, fragmented, and porous structures at higher acid concentrations. These microstructural transformations provide direct evidence of enhanced apatite decomposition and increased REE liberation, explaining the substantial improvement in extraction efficiency. The strong correlation between acid-induced microstructural evolution and REE recovery demonstrates that hydrochloric acid concentration is the primary driving force governing leaching performance. This study provides new mechanistic insight into acid-assisted apatite dissolution and establishes an optimized, economically attractive strategy for the efficient recovery of valuable REEs from apatite-rich iron ore tailings.

KEYWORDS

Rare earth elements
Leaching
Hydrochloric acid
Apatite concentrate
SEM

OPEN ACCESS

1. Introduction

Rare earth elements (REEs) are recognized as strategically critical minerals owing to their indispensable contribution to the development and deployment of advanced technologies such as high-performance batteries, permanent magnetic materials, and defense-related systems [1–3]. According to the classification reported by Ford et al. [1], the

* Corresponding author. *E-mail address:* erfan.mohamadzadeh22@sharif.edu (E. Mohammadzadeh)
Received 14 March 2026; Received in revised form 30 May 2026; Accepted 2 June 2026.

https://doi.org/10.53063/synsint.2026.62335

rare earth family comprises fifteen lanthanide metals La, Ce, Pr, Nd, Pm, Sm, Eu, Gd, Tb, Dy, Ho, Er, Tm, Yb, and Lu together with yttrium (Y) and scandium (Sc). From a geochemical and industrial perspective, these elements are commonly divided into light rare earth elements (LREEs), spanning from La to Gd, and heavy rare earth elements (HREEs), which include Tb through Lu as well as Ford and co-workers [1] further highlighted that REEs constitute a group of strategic resources that are fundamental to enabling the global transition toward low-carbon and sustainable energy systems, particularly because of their essential role in next-generation battery technologies [4]. The growing scientific and industrial interest in rare earth elements stems from their exceptional magnetic, optical, and electronic characteristics. Although these elements were historically utilized primarily in glass production, their functional relevance has expanded significantly into fast-growing technological sectors, including energy storage devices and high-strength permanent magnets. The sharp increase in global demand for REEs has therefore intensified the necessity to identify and develop alternative and non-conventional sources for their recovery and supply [5]. Modern technological progress is deeply intertwined with the availability of rare earth metals. Their critical importance is reflected in their extensive application across a wide spectrum of contemporary products, such as smartphones, computers, televisions, hybrid and electric vehicles, wind energy systems, photovoltaic technologies, and data storage devices. The widespread reliance of these technologies on REEs clearly demonstrates their fundamental role in sustaining present-day industrial and digital infrastructure [6–11]. From a mineralogical standpoint, lanthanides are predominantly extracted from rare earth–bearing minerals including bastnäsite, monazite, xenotime, and fluocerite, which constitute the principal feedstocks for industrial-scale REE production. In addition to rare earths, phosphorus, despite its relatively low abundance in the Earth's crust, is an element of critical importance due to its essential function in biological systems and its extensive utilization in agricultural, medical, and industrial applications. Phosphorus-derived products such as monoammonium phosphate, diammonium phosphate, and triple superphosphate are typically manufactured using phosphoric acid (H_3PO_4). Consequently, the rising global demand for phosphate fertilizers has led to a parallel increase in phosphoric acid production. Apatite, a phosphate-rich mineral, has long been employed as the primary raw material for phosphorus recovery, particularly in fertilizer and animal feed industries. In this context, wet-process phosphoric acid (WPA) represents a key intermediate product, which is commonly produced through the acid digestion of apatite concentrate [12, 13]. The distribution profile of rare earth elements within the apatite concentrate, along with their relative concentrations, is presented in Fig. 1 [14].

Apatite concentrate (AP), obtained via a combination of physical and physicochemical processing of phosphate ores, generally contains rare earth elements (REEs) at levels ranging from approximately 0.1 to 1.5 wt%. Despite the relatively modest concentration of REEs in AP, the enormous worldwide reserves of phosphate rock render this material a promising and sustainable secondary resource for rare earth recovery [15]. Consequently, numerous approaches have been investigated to extract REEs from apatite-based materials [16, 17], with acid leaching being one of the most extensively studied techniques [18]. Recent research has focused on optimizing the acid leaching of a rare earth–bearing apatite ore sourced from Mongolia. This ore exhibited a relatively high total rare earth oxide (TREO) content of approximately 10%, while also containing substantial quantities of impurity phases, notably calcium (about 33% as CaO) and iron (around 23% as Fe_2O_3). To mitigate the adverse impact of iron during leaching, magnetic separation was initially employed to remove iron-rich minerals. Subsequent leaching experiments systematically examined the influence of key operational parameters, including acid type, acid concentration, temperature, and solution pH, on the efficiency of REE extraction. Among the acids evaluated, hydrochloric acid demonstrated superior performance, enabling the dissolution of more than 90% of the rare earth elements within a one-hour leaching period. Nevertheless, the extensive co-dissolution of calcium posed challenges for downstream REE separation and purification. To overcome this limitation, a two-step leaching process was proposed. In the first stage, calcium was selectively dissolved using a dilute hydrochloric acid solution (1.0 M HCl), followed by a second leaching stage employing a higher acid concentration (2.0 M HCl) to extract the REEs. This

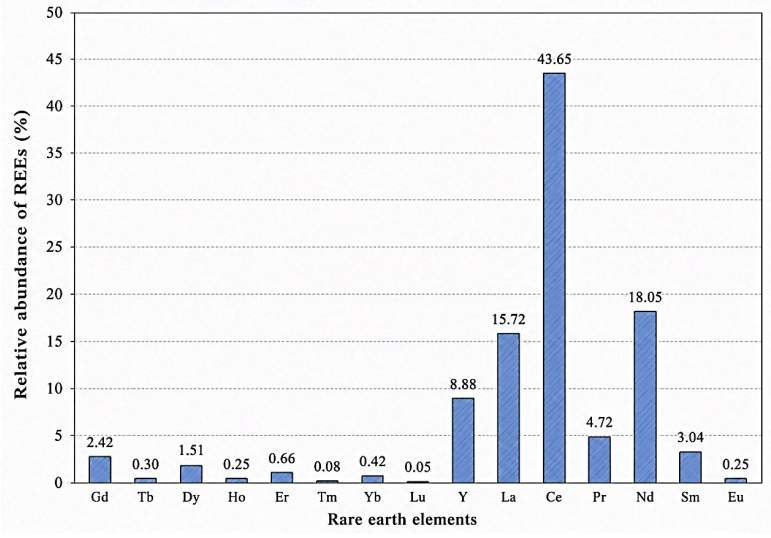

Fig. 1. REE distribution in apatite concentrate.

sequential approach effectively reduced the calcium content in the leachate while maintaining a high recovery efficiency for rare earth elements [19]. In general, apatite ores are commonly decomposed using inorganic acids such as hydrochloric acid (HCl), sulfuric acid (H_2SO_4), and nitric acid (HNO_3) [16]. The chemical reactions governing the apatite decomposition process are represented by Eq 1:

$$Ca_5(PO_4)_3F+5H_2SO_4+nH_3PO_4\rightarrow(n+3)H_3PO_4+5CaSO_4.mH_2O+HF \quad (1)$$

During sulfuric acid (H_2SO_4) leaching, a substantial proportion of rare earth elements, approximately 75%, remains immobilized in the solid residue as a result of gypsum ($CaSO_4.2H_2O$) formation, which exhibits very limited solubility. By contrast, employing nitric acid (HNO_3) or hydrochloric acid (HCl) as the leaching medium markedly enhances REE dissolution, with overall extraction efficiencies exceeding 80%. Stone et al. [20] systematically evaluated the leaching behavior of rare earth elements from fluorapatite and rare earth phosphate concentrates using several acidic systems, including H_2SO_4, HCl, HNO_3, and H_3PO_4, to identify the most effective leachant for REE recovery. Their results demonstrated that phosphoric acid (H_3PO_4) exhibited the weakest leaching capability among the acids investigated. In contrast, nitric acid achieved the highest extraction performance, yielding recoveries of 78.6% for La, 83.0% for Ce, and 79.7% for Nd [21]. As illustrated in Fig. 2, complete dissolution of calcium was achieved when HCl and HNO_3 were used as leaching agents, whereas calcium leaching in phosphoric acid was limited to approximately 85% [9].

Among the commonly used mineral acids, hydrochloric acid (HCl) demonstrates marked advantages over sulfuric acid (H_2SO_4) and nitric acid (HNO_3) for the extraction of rare earth elements (Ce, La, and Nd) from calcium-rich, apatite-type ores. In contrast to H_2SO_4, which promotes the formation of insoluble gypsum ($CaSO_4.2H_2O$) and consequently immobilizes a significant fraction of REEs within the solid residue, HCl maintains calcium in solution as Ca^{2+} ions and facilitates the formation of soluble REE–chloride complexes. This behavior effectively suppresses co-precipitation phenomena and substantially improves rare earth recovery. Although nitric acid also prevents gypsum precipitation, its application is associated with several drawbacks, including the evolution of hazardous NO_x gases and accelerated corrosion of processing equipment, both of which impose serious constraints on large-scale industrial implementation. In comparison, hydrochloric acid enables rapid dissolution kinetics, frequently achieving rare earth recoveries exceeding 90% within one hour at ambient temperature, as reported by some researchers for Mongolian apatite-derived ores [19, 22]. Furthermore, HCl exhibits significantly superior leaching performance relative to phosphoric acid (H_3PO_4), which displays limited dissolution efficiency due to its weaker acidity and the tendency for complex secondary precipitation reactions [23]. An additional advantage of hydrochloric acid lies in its suitability for selective, multi-stage leaching strategies, wherein calcium can be preferentially removed before rare earth extraction, thereby simplifying subsequent purification steps. Considering its high extraction efficiency, reduced formation of secondary precipitates, relatively manageable operational risks, and strong compatibility with established hydrometallurgical processes, hydrochloric acid was selected as the leaching agent in the present study. Accordingly, apatite samples were leached using HCl, and the effects of key operational variables, including acid concentration, solid-to-liquid (S/L) ratio, and leaching duration, were systematically examined. To quantitatively assess and optimize leaching performance, response surface methodology (RSM) was integrated with a design of experiments (DOE) framework, allowing the individual and interactive effects of process parameters to be evaluated and the optimal conditions for maximum rare earth recovery to be determined.

2. Experimental

2.1. Materials and apparatus

The apatite concentrate used throughout this investigation was obtained from the beneficiation plant of the Chadormalu Iron Ore Complex, Iran. The received material possessed a particle size below 50 μm and was utilized directly in the leaching experiments without any additional comminution or grinding. Hydrochloric acid (HCl, analytical grade, Merck) was employed as the leaching agent in all experiments. The concentrations of rare earth elements (REEs) in the untreated apatite concentrate were determined by inductively coupled plasma mass spectrometry (ICP-MS), whereas the elemental composition of the leach solutions was measured using inductively coupled plasma atomic emission spectroscopy (ICP-AES). The chemical composition of the major constituents in the apatite concentrate, as determined by ICP-OES analysis, is summarized in Table 1.

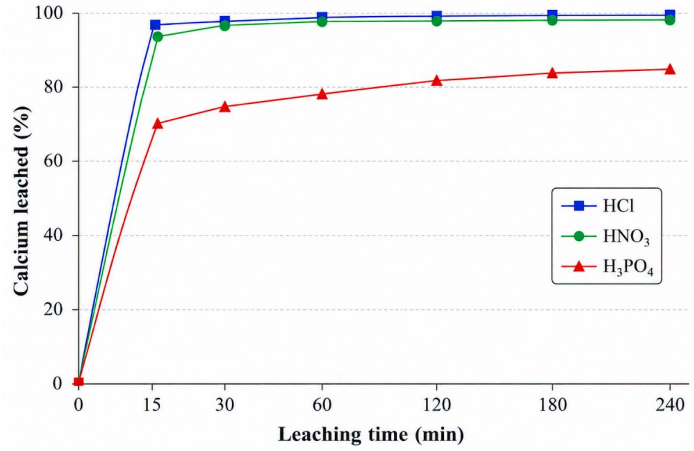

Fig. 2. Calcium leaching curves of the concentrate in different acids.

Table 1. ICP-MS analysis of rare earth elements in the apatite concentrate.

Rare earth element	Symbol	Concentration (ppm)
Scandium	Sc	1.40
Yttrium	Y	655.50
Lanthanum	La	1551.00
Cerium	Ce	3707.00
Praseodymium	Pr	559.27
Neodymium	Nd	1832.20
Samarium	Sm	277.48
Europium	Eu	26.37
Gadolinium	Gd	219.66
Terbium	Tb	28.30
Dysprosium	Dy	136.80
Erbium	Er	62.81
Thulium	Tm	7.10
Ytterbium	Yb	40.10
Lutetium	Lu	4.49

2.2. Leaching experiments

Leaching experiments were performed in a 200 ml three-neck glass reactor fitted with a magnetic stirrer and a heating system to evaluate the effect of temperature on the dissolution of rare earth elements (REEs). According to the experimental conditions summarized in Table 2, the leaching process was carried out under magnetic agitation at a controlled temperature of 65 °C.

Leaching tests were carried out in a 200 ml glass reactor fitted with a magnetic stirrer and a heating system to evaluate the influence of temperature on the extraction of rare earth elements (REEs). Temperature is widely recognized as one of the most influential operating variables in hydrometallurgical leaching because it directly affects both reaction kinetics and mass transfer. Previous investigations have demonstrated that raising the temperature from 298 K (25 °C) to 348 K (75 °C) increased REE recovery from approximately 35% to 75% after two hours of leaching. Such a pronounced improvement indicates that the dissolution of rare earth elements is strongly promoted by thermal activation, particularly for light rare earth elements (LREEs), which exhibit greater sensitivity to temperature changes. These observations further suggest that, under these operating conditions, the overall leaching rate is predominantly controlled by surface chemical reactions rather than by diffusion or external mass transfer limitations [24]. The beneficial effect of temperature has also been confirmed in studies involving mechanically activated leaching systems. For example, mechanical milling performed at 80 °C for 60 min increased the REE extraction efficiency from 48.6% to 88.4%. Simultaneously, the apparent activation energy decreased from 83.9 to 37.4 $kJ.mol^{-1}$, indicating a shift in the rate-limiting mechanism from chemical reaction control toward diffusion-controlled kinetics [25]. The significance of thermal conditions has likewise been reported for the recovery of rare earth elements from secondary resources. In the sulfuric acid leaching of end-of-life smartphone components, the dissolution behavior of dysprosium (Dy), neodymium (Nd), and praseodymium (Pr) exhibited a non-linear temperature dependence. Extraction efficiency initially decreased between approximately 20 and 46 °C but increased substantially at higher temperatures, reaching its maximum near 80 °C. The highest recoveries were achieved using a dilute sulfuric acid solution (0.2 M), a leaching time of about 150 min, and an operating temperature close to 80 °C. These findings demonstrate the complex kinetics governing REE dissolution and emphasize that maintaining an appropriate temperature, particularly within the range of 50–80 °C, is essential for efficient metal recovery from electronic waste [26]. Similar observations have been reported for phosphogypsum (PG), where the effects of acid concentration, solid-to-liquid (S/L) ratio, and temperature were investigated using citric acid and sulfuric acid as leaching agents. Initial factorial experiments conducted with 3 M H_2SO_4 at 80 °C produced REE recoveries approaching 90%. However, subsequent optimization using Response Surface Methodology (RSM) demonstrated that comparable extraction efficiencies could be obtained at a considerably lower temperature of 55 °C by employing 2.9 M sulfuric acid and an S/L ratio of 1.7:20 for only 20 min. These results indicate that efficient REE extraction can be achieved under moderate thermal conditions, thereby lowering energy requirements while simultaneously reducing acid consumption and operating costs [27]. The role of temperature was further investigated through an RSM-based central composite design (CCD) study on citric acid leaching of phosphogypsum. In that work, temperature, acid concentration, and leaching time were optimized simultaneously. Maximum REE dissolution (90.1%) was obtained at 2 M citric acid, 343 K (70 °C), and a reaction time of 180 min. Kinetic evaluation revealed that diffusion became the dominant rate-controlling mechanism as temperature increased, confirming that thermal activation substantially enhances REE release. The authors concluded that operating near 70 °C provides an effective balance between extraction efficiency, energy consumption, and environmental sustainability [28]. Further evidence supporting the importance of temperature was reported in a systematic investigation of sulfuric acid leaching of phosphogypsum, where the effects of particle size, acid concentration, temperature, and redox additives were evaluated. Under elevated-temperature conditions (above approximately 50 °C), overall REE recoveries reached nearly 99%, with lanthanum exhibiting almost complete dissolution. The remaining rare earth elements followed similar trends, although with slightly lower extraction efficiencies. These findings highlight the positive influence of temperature on phosphogypsum dissolution and demonstrate its potential for improving process performance during pilot- and industrial-scale applications [29]. Based on the collective findings reported in the

Table 2. Test conditions.

Parameter	Description
Reactor type	200 ml glass reactor
Stirring method	Magnetic stirring
Heating method	Equipped with a heater
Temperature	25–65 °C
Agitation type	Magnetic agitation
Purpose	To investigate the influence of temperature on the dissolution behavior of rare earth elements (REEs)

literature, the experimental temperature interval selected for the present investigation was 25–65 °C. Accordingly, the leaching apparatus and experimental design were configured to operate reliably throughout this temperature range. The leaching time and solid-to-liquid ratio were selected based on preliminary optimization considerations and published studies reporting suitable operating conditions for hydrochloric acid leaching of apatite-derived rare earth elements. Accordingly, a leaching time of 60 min and a solid-to-liquid ratio of 1:9 were adopted as fixed experimental conditions throughout the statistical design, allowing the optimization procedure to focus exclusively on the effects of hydrochloric acid concentration and leaching temperature.

2.3. Design of experiments (DOE)

Recent investigations have confirmed the effectiveness of Response Surface Methodology (RSM), especially when implemented through central composite design (CCD), as a reliable statistical tool for optimizing multivariable engineering processes. In cement-based material design, CCD has been successfully applied to characterize nonlinear relationships and interaction effects among formulation variables while substantially decreasing the experimental workload. Likewise, in studies involving heat transfer enhancement using nanofluids, CCD-assisted RSM has demonstrated excellent predictive capability by accurately representing response curvature and variable interactions with a relatively limited number of experimental trials. These studies consistently indicate that CCD facilitates the development of statistically significant second-order regression models capable of describing complex process behavior with high accuracy. Consequently, the RSM CCD approach has become a widely adopted, economical, and efficient optimization technique across numerous scientific and engineering disciplines [30, 31]. In the present work, the experimental program was designed using a central composite design (CCD) to systematically investigate the leaching process. Hydrochloric acid concentration and leaching temperature were selected as the independent (input) variables, and their corresponding levels are summarized in Table 3. To clearly evaluate the effects of these operating parameters on the extraction of individual rare earth elements, the experimental matrix together with the measured leaching efficiencies for each element is presented separately. Throughout all experimental runs, the solid-to-liquid (S/L) ratio and the leaching time were maintained at fixed values, as specified in the experimental design.

The leaching efficiencies of lanthanum (La), cerium (Ce), and neodymium (Nd) were selected as the response variables in the statistical analysis. A central composite design (CCD) was employed in which the hydrochloric acid concentration was investigated over a range of 2.0–13.6 M, while the solid-to-liquid (S/L) ratio and leaching time were fixed at 1:9 and 60 min, respectively, throughout all experimental runs. The experimental responses were correlated using a second-order polynomial regression model, expressed as:

Table 3. Experimental variables and their corresponding levels employed in the RSM design.

Factor	Code	Low level	High level	Unit
HCl concentration	M	2.0	13.6	M
Leaching temperature	T	25	65	°C

$$X_i = \beta_0 + A\beta_1 + B\beta_2 + Ab\beta_{12} + \beta_{11}A^2 + \beta_{22}B^2 \quad (2)$$

where X_i represents the predicted leaching recovery, A and B denote the hydrochloric acid concentration and leaching temperature, respectively, and β_0, β_1, β_2, β_{12}, β_{11}, and β_{22} are the regression coefficients corresponding to the intercept, linear, interaction, and quadratic terms of the model. Statistical analysis of the experimental data, including analysis of variance (ANOVA) and the generation of three-dimensional response surface plots, was performed using Design-Expert software (Version 13, Stat-Ease Inc., Minneapolis, MN, USA). The optimum operating conditions for maximizing rare earth element recovery were determined using the software's numerical optimization algorithm in conjunction with graphical response surface analysis. It should be noted that only hydrochloric acid concentration and leaching temperature were incorporated into the central composite design as independent variables for statistical evaluation. The solid-to-liquid ratio (1:9) and the leaching time (60 min) were intentionally maintained at fixed values throughout all experiments in order to isolate the individual and combined effects of the selected factors. This experimental strategy reduced unnecessary variability and enabled a more reliable interpretation of the response surface model within the investigated design space.

3. Results and discussion

3.1. Analysis

The concentrations of rare earth elements determined for the apatite concentrate are presented in Table 1. The results demonstrate that La, Ce, and Nd are the predominant rare earth elements, collectively representing more than 77% of the total REE content. This compositional distribution justifies the selection of these three elements as the primary targets for the subsequent leaching and optimization studies.

3.2. Response analysis and interpretation

To investigate the relationship between the operating conditions and the recovery of rare earth elements, the experimental program was designed using a central composite design (CCD). Because the solid-to-liquid ratio and leaching duration remained constant during the experimental program, the statistical analysis and response surface models exclusively describe the influence of hydrochloric acid concentration and leaching temperature on rare earth element recovery. Consequently, all regression equations and graphical interpretations presented in the following sections should be considered within the experimental domain defined by these two independent variables. The resulting design matrix and the measured leaching efficiencies for La, Ce, and Nd are presented in Table 4. To further interpret the experimental observations, response surface plots together with the corresponding ANOVA results are presented for each response, allowing both the individual and interaction effects of the process variables to be systematically evaluated. In all experiments, the leaching duration and the solid-to-liquid ratio were kept constant at 60 min and 1:9, respectively.

To identify the regression model that best described the experimental responses, several polynomial models, namely the mean, linear, two-factor interaction (2FI), quadratic, and cubic models, were examined using Design-Expert software. Model selection was performed by

Table 4. ICP-OES-determined leaching recoveries of cerium (Ce), lanthanum (La), and neodymium (Nd) at 25 and 65 °C.

Exp. No.	HCl concentration (M)	Temperature (°C)	Ce recovery (%)	La recovery (%)	Nd recovery (%)
1	2.0	25	3.50	4.63	4.36
2	2.0	65	5.01	4.71	4.40
3	3.0	25	67.06	61.33	66.11
4	3.0	65	70.10	77.27	67.01
5	3.5	25	69.20	67.58	67.22
6	3.5	65	75.43	77.35	68.04
7	4.0	25	80.12	76.22	67.45
8	4.0	65	82.78	77.53	68.02
9	4.2	25	80.67	76.56	67.57
10	4.2	65	85.12	77.60	69.01
11	5.0	25	82.01	77.11	68.01
12	5.0	65	86.04	78.03	70.33
13	5.7	25	83.22	78.01	69.66
14	5.7	65	87.65	78.60	71.77
15	6.0	25	85.47	74.78	70.42
16	6.0	65	90.55	80.14	72.40
17	6.5	25	86.02	78.02	70.55
18	6.5	65	91.22	78.60	72.77
19	7.0	25	86.65	78.79	71.01
20	7.0	65	91.88	79.11	72.55
21	8.0	25	86.64	79.17	70.67
22	8.0	65	92.10	81.33	72.88
23	8.4	25	87.01	80.11	71.44
24	8.4	65	91.05	81.50	72.90
25	9.0	25	88.33	80.46	72.55
26	9.0	65	92.13	82.03	73.01
27	10.0	25	89.66	81.02	73.15
28	10.0	65	92.10	82.50	73.45
29	11.0	25	89.02	82.22	74.45
30	11.0	65	93.12	83.44	74.22
31	12.0	25	91.43	84.12	75.66
32	12.0	65	92.85	84.88	75.88
33	13.6	25	92.12	86.03	76.01
34	13.6	65	94.19	86.33	76.34

comparing the corresponding sum of squares values. Based on this evaluation, the quadratic model was found to provide the most appropriate fit for the experimental data. The corresponding ANOVA results for the quadratic models developed for Ce, La, and Nd leaching recoveries are presented in Tables 5, 6, and 8, respectively.

3.2.1. Statistical analysis of ANOVA in cerium extraction

The adequacy of the developed regression model was assessed using analysis of variance (ANOVA), in which the F-value and p-value serve as the primary statistical indicators of model significance. The F-value evaluates the extent to which the regression model explains the observed variation in the response variable relative to the unexplained residual error, whereas the p-value represents the probability that the observed relationship has arisen by chance. In general, regression models with relatively high F-values and p-values below 0.05 are considered statistically significant, indicating that the independent variables exert a meaningful influence on the response and that the null hypothesis can be rejected [32]. The ANOVA results for the Ce recovery model are summarized in Table 5. The developed model exhibited an F-value of 9.28 together with a p-value of 0.0007,

confirming that the regression equation is statistically significant. This result indicates that there is only a 0.07% probability that the observed model performance could be attributed to random experimental variation. Examination of the individual model terms further revealed that hydrochloric acid concentration (factor A) had a statistically significant effect on Ce recovery ($p < 0.05$), whereas the effect of temperature (factor B) was not statistically significant within the investigated experimental domain ($p > 0.05$). These findings demonstrate that variations in acid concentration contributed much more strongly to cerium extraction than changes in temperature over the selected operating range. From a modeling perspective, retaining only statistically meaningful terms generally improves model robustness and predictive capability. Therefore, insignificant terms that are not required to preserve the hierarchical structure of the regression model may be omitted to obtain a more parsimonious model without compromising its predictive performance.

The statistical adequacy of the regression model developed for Ce recovery was evaluated using ANOVA, and the corresponding results are summarized in Table 4. The ANOVA indicated that the proposed model was statistically significant, as demonstrated by a Model F-value of 9.28 and a p-value of 0.0007. This result implies that there is only a 0.07% probability that the observed relationship between the process variables and the response occurred due to random experimental noise. The regression model exhibited a sum of squares (SS) of 5309.93, while the residual sum of squares was 8866.30, resulting in a total sum of squares of 14176.23. These statistical parameters confirm that the model adequately describes the relationship between the selected operating variables and cerium recovery within the investigated experimental region. A detailed examination of the individual model terms revealed that hydrochloric acid concentration (factor A) was the dominant variable affecting cerium extraction. This factor produced an F-value of 18.13 together with a p-value of 0.0002, confirming its highly significant contribution to the model. The large F-value and very low probability indicate that increasing the acid concentration has a pronounced and statistically meaningful effect on the dissolution of cerium, making it the principal parameter governing the leaching process. In contrast, temperature (factor B) exhibited an F-value of 0.437 and a p-value of 0.5134, indicating that its influence was not statistically significant within the investigated temperature range of 25–65 °C. Although elevated temperatures generally promote reaction kinetics, the present results suggest that, under the selected experimental conditions, variations in hydrochloric acid concentration exert a considerably greater influence on cerium recovery than temperature. The regression equation generated by the Design-Expert software for predicting cerium recovery is expressed as:

$$\text{Ce recovery (\%)} = 84.23 + 17.45A + 7.17B \quad (3)$$

where A and B represent the coded values of hydrochloric acid concentration and leaching temperature, respectively. The intercept (84.23) corresponds to the predicted cerium recovery at the center point of the experimental design. The positive regression coefficient associated with acid concentration (+17.45) indicates that increasing the HCl concentration produces a substantial enhancement in cerium extraction, whereas the smaller positive coefficient for temperature (+7.17) suggests a comparatively weaker contribution. These observations are in excellent agreement with the ANOVA results, which identified acid concentration as the primary factor controlling the leaching behavior. Overall, the statistical analysis confirms that the developed regression model provides a reliable description of cerium recovery within the investigated design space. Although both operating variables positively influence the extraction process according to the regression equation, the ANOVA results clearly demonstrate that hydrochloric acid concentration is the only statistically significant factor, whereas the effect of temperature is comparatively limited. The three-dimensional response surface generated from the fitted model, illustrating the combined influence of hydrochloric acid concentration and temperature on cerium recovery, is presented in Fig. 3.

Fig. 3 presents the three-dimensional response surface together with the corresponding standard error distribution, illustrating the combined influence of hydrochloric acid concentration (A) and leaching temperature (B) on Ce recovery. The response surface demonstrates that the extraction efficiency of Ce increases progressively with increasing acid concentration, whereas the effect of temperature is comparatively less pronounced. The upward trend of the surface indicates that higher hydrochloric acid molarity promotes the dissolution of cerium, resulting in improved leaching performance. The highest extraction efficiencies, exceeding 90%, are predicted in the region corresponding to the maximum acid concentration and elevated temperature, indicating that these operating conditions are the most favorable for Ce recovery within the investigated experimental domain. The accompanying standard error surface provides valuable information regarding the reliability of the developed regression model throughout the design space. As expected for a well-constructed response surface model, the prediction error is lowest around the central region of the experimental design, where the density of experimental data is greatest. Conversely, the standard error gradually increases toward the boundaries of the design space because fewer experimental observations are available in these regions. Consequently, predictions generated near the center of the design are associated with greater confidence, whereas those approaching the experimental limits should be interpreted more cautiously. A comparison of the two

Table 5. ANOVA results of the quadratic regression model developed for cerium (Ce) recovery.

ANOVA term	SS	DOF	MS	F	p-value	Interpretation
Quadratic model	5309.93	2	2654.97	9.28	0.0007	Statistically significant
Acid concentration (A)	5184.94	1	5184.94	18.13	0.0002	Significant factor
Temperature (B)	124.99	1	124.99	0.437	0.5134	Not significant
Residual error	8866.30	31	286.01	—	—	—
Total variation	14176.23	33	—	—	—	—

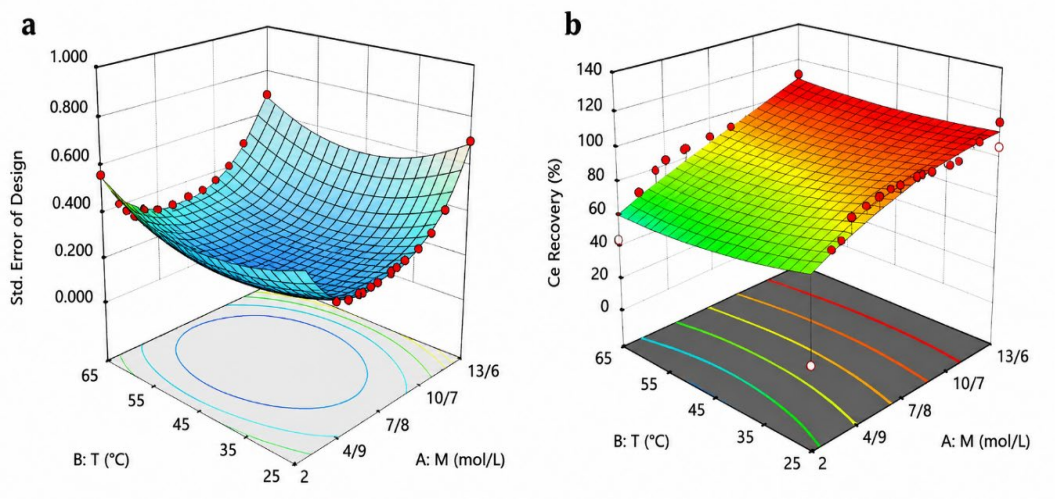

Fig. 3. a) Standard error distribution over the experimental design domain and b) three-dimensional response surface illustrating the recovery of cerium.

surfaces further confirms the adequacy of the statistical model. The region associated with the highest predicted cerium recovery also corresponds to relatively low prediction uncertainty, demonstrating that the optimized operating conditions are supported by a reliable regression model. These findings indicate that increasing hydrochloric acid concentration is the primary factor governing Ce extraction, while temperature plays a secondary role within the investigated range. Overall, the response surface analysis demonstrates that the developed model can effectively predict cerium recovery and provides a useful basis for determining optimal leaching conditions.

3.2.2. ANOVA analysis for the leaching of lanthanum

ANOVA was performed to assess the adequacy of the linear regression model proposed for predicting La leaching recovery. The model correlates the extraction efficiency with two independent process variables, including hydrochloric acid concentration (factor A) and leaching temperature (factor B). Statistical significance was determined by comparing the calculated F-values with their corresponding p-values, allowing the contribution of each factor to be quantitatively evaluated.

The statistical results obtained from the ANOVA confirm that the developed regression model adequately describes the leaching behavior of La. The model was found to be statistically significant, with an F-value of 7.28 and a corresponding p-value of 0.0026, indicating that the relationship between the selected process variables and La recovery is unlikely to have arisen by chance. These statistical indicators demonstrate that the model provides a reliable framework for evaluating the influence of the investigated operating conditions within the experimental domain. Among the investigated variables, hydrochloric acid concentration (factor A) exerted the strongest influence on lanthanum recovery. The ANOVA results yielded an F-value of 14.31 together with a p-value of 0.0007, confirming that acid concentration is a highly significant parameter affecting the dissolution of lanthanum-bearing phases. The sum of squares attributed to this factor (3495.28) accounts for approximately 98.3% of the total variation explained by the regression model (3554.29), demonstrating that variations in acid molarity dominate the extraction process. Increasing the concentration of hydrochloric acid therefore substantially enhances lanthanum dissolution by promoting the breakdown of the apatite matrix and facilitating the release of rare earth elements into the leaching solution. Conversely, leaching temperature (factor B) exhibited only a limited influence on La recovery. The corresponding F-value (0.2416) and p-value (0.6265) indicate that the temperature effect is not statistically significant over the investigated range of 25–65 °C. Moreover, the relatively small sum of squares associated with this factor (59.00) suggests that temperature contributes only marginally to the variability in lanthanum extraction. These findings imply that the leaching process is governed predominantly by acid availability rather than thermal activation under the selected experimental conditions. The residual variation, represented by a sum of squares of 7570.31, reflects the portion of the experimental response that is not explained by the present linear model. Nevertheless, the regression model accounts for approximately 32% of the overall variation in lanthanum recovery, indicating an acceptable predictive capability for identifying general process trends. Although the model successfully captures the principal effect of acid concentration, the inclusion of higher-order or interaction terms in future investigations may further improve its predictive accuracy and better describe the complexity of the leaching mechanism. Based on the regression coefficients generated by the Design-Expert software, the recovery of lanthanum can be expressed by the following coded linear equation:

$$\text{La recovery (\%)} = 77.15 + 18.20A + 1.32B \quad (4)$$

where A and B denote the coded values of hydrochloric acid concentration and leaching temperature, respectively. The intercept (77.15) represents the predicted lanthanum recovery at the center point of the experimental design. The coefficient associated with acid concentration (+18.20) indicates that increasing hydrochloric acid concentration produces a substantial improvement in La extraction, which is fully consistent with the ANOVA results. In comparison, the coefficient assigned to temperature (+1.32) is considerably smaller, confirming its relatively minor contribution to the overall recovery. The reliability of these regression coefficients is further supported by the corresponding 95% confidence intervals. The confidence interval for factor A ranges from 8.39 to 28.01, excluding zero and therefore confirming the statistical significance of acid concentration. In contrast,

Table 6. Analysis of variance (ANOVA) for the quadratic regression model of lanthanum (La) recovery.

ANOVA term	df	Sum of squares (SS)	Mean square (MS)	F-statistic	p-value	Statistical interpretation
Regression model	2	3554.29	1777.14	7.28	0.0026	Significant
Hydrochloric acid concentration (A)	1	3495.28	3495.28	14.31	0.0007	Significant
Leaching temperature (B)	1	59.00	59.00	0.2416	0.6265	Not significant
Residual error	31	7570.31	244.20	—	—	—
Total variation	33	11124.60	—	—	—	—

the confidence interval for Factor B extends from -4.15 to 6.78, encompassing zero and indicating that temperature does not significantly influence lanthanum recovery at the 95% confidence level. Collectively, these statistical results demonstrate that hydrochloric acid concentration is the principal factor controlling lanthanum leaching, whereas the effect of temperature remains negligible within the investigated operating conditions.

The developed regression model demonstrates that variations in hydrochloric acid concentration predominantly control the extraction of lanthanum, while temperature has no statistically significant contribution under the examined experimental conditions. Despite the limited effect of temperature, it was maintained in the final regression model since the overall model exhibited statistical significance according to the ANOVA analysis ($p = 0.0026$).

The graphical outputs generated by the Design-Expert software are presented in Fig. 4, providing a visual interpretation of the developed response surface model for La recovery. Fig. 6a illustrates the distribution of the model prediction error throughout the experimental region. In contrast, Fig. 4b depicts the corresponding response surface describing the influence of hydrochloric acid concentration and leaching temperature on La extraction efficiency. The prediction error surface shown in Fig. 4a indicates that the lowest uncertainty is concentrated in the central portion of the experimental domain, corresponding to hydrochloric acid concentrations between 4 and 9 M and temperatures between 35 and 55 °C. This region represents the area where the regression model provides its highest predictive reliability, owing to the greater density of experimental information associated with the central composite design (CCD). Moving toward the edges of the design space, particularly under the lowest and highest operating conditions, the standard error gradually increases. Such behavior is characteristic of response surface models and indicates that predictions near the design boundaries should be interpreted with greater caution because of increased extrapolation uncertainty. The three-dimensional response surface shown in Fig. 4b illustrates the variation of lanthanum recovery as a function of hydrochloric acid concentration and leaching temperature. A continuous increase in La extraction is observed with increasing acid concentration across the investigated operating range. Under relatively dilute acid conditions (approximately 2–4 M), lanthanum recovery remains limited, whereas substantially higher recoveries are obtained as the hydrochloric acid concentration approaches the upper levels investigated. The maximum recovery, exceeding 86%, is achieved at the highest acid concentration employed in this study. This behavior confirms that hydrochloric acid concentration is the dominant process variable governing the dissolution of lanthanum-bearing phases, which is in excellent agreement with the ANOVA results showing a statistically significant contribution of acid concentration ($F = 14.31$, $p = 0.0007$). Although the response surface exhibits a slight upward trend with increasing temperature, the statistical analysis indicates that this variable does not significantly affect lanthanum recovery within the investigated range of 25–65 °C ($F = 0.2416$, $p = 0.6265$). Consequently, the observed improvement at elevated temperatures should be interpreted as a

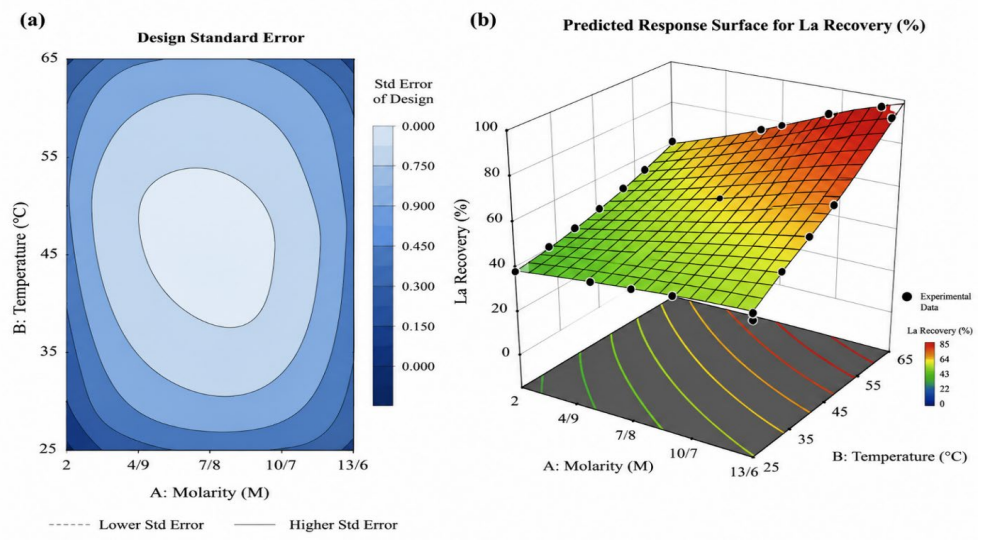

Fig. 4. a) Design standard error surface and b) three-dimensional response surface for lanthanum (La) recovery.

Table 7. Regression coefficients and statistical evaluation of the developed model for lanthanum (La) recovery.

Regression term	Estimate	Standard deviation	95% confidence bounds	Statistical interpretation
Constant term	77.15	2.76	71.52 to 82.78	—
Acid concentration (A)	18.20	4.81	8.39 to 28.01	Significant effect
Temperature (B)	1.32	2.68	-4.15 to 6.78	No significant effect

secondary effect rather than the principal driving force of the leaching process. The relatively gentle slope of the response surface along the temperature axis further supports this conclusion, indicating that variations in acid concentration have a much greater influence on extraction efficiency than temperature changes. Overall, the graphical analysis is fully consistent with the regression model and ANOVA results. The response surface confirms that hydrochloric acid concentration is the primary parameter controlling lanthanum dissolution, while the contribution of temperature remains comparatively limited under the investigated conditions. Furthermore, the low prediction error observed over the central experimental region demonstrates the robustness of the developed model and supports its suitability for process optimization within the selected operating domain. The recovery behavior obtained for lanthanum also follows the same general trend observed for the other investigated rare earth elements, indicating that the developed leaching strategy applies to the simultaneous extraction of Ce, La, and Nd from the apatite concentrate.

3.2.3. ANOVA analysis for the leaching of neodymium

Table 8 summarizes the ANOVA for the regression model established to predict Nd recovery. The statistical evaluation was carried out in Design-Expert software to determine the individual effects of hydrochloric acid concentration (A) and leaching temperature (B) on Nd leaching performance.

The ANOVA results demonstrate that the developed regression model provides a statistically reliable description of Nd recovery under the investigated experimental conditions. The overall model yielded an F-value of 6.14 with a corresponding p-value of 0.0057, confirming that the regression is statistically significant. The probability that this relationship arose solely from random experimental error is therefore only 0.57%, indicating that the selected model adequately represents the dependence of Nd recovery on the investigated process variables. Among the evaluated factors, hydrochloric acid concentration (factor A) was identified as the primary variable controlling neodymium extraction. This factor produced an F-value of 12.23 together with a p-value of 0.0014, confirming its highly significant contribution to the regression model. The corresponding sum of squares (2458.61) represents nearly the entire variation explained by the model (2468.88), demonstrating that changes in acid concentration exert a dominant influence on the dissolution of neodymium-bearing mineral phases. Increasing hydrochloric acid concentration, therefore, results in a substantial improvement in Nd recovery throughout the investigated operating range. By contrast, leaching temperature (factor B) exhibited only a negligible influence on the extraction process. The calculated F-value of 0.0511 and the associated p-value of 0.8226 indicate that temperature does not significantly affect neodymium recovery within the experimental interval of 25–65 °C. Furthermore, the relatively small sum of squares assigned to this factor (10.27) confirms that its contribution to the overall response variability is minimal compared with that of hydrochloric acid concentration. The residual variation, represented by a sum of squares of 6230.38, reflects the fraction of the experimental variability that is not explained by the present regression model. Although the developed model successfully captures the principal effect governing neodymium dissolution, the remaining unexplained variance suggests that additional higher-order terms or factor interactions could further improve the predictive capability of future models. Nevertheless, the current regression model provides a statistically valid description of the experimental data and is suitable for evaluating the influence of the selected operating variables. Based on the regression coefficients generated by Design-Expert software, the recovery of neodymium can be expressed by the following linear equation in terms of the coded variables:

$$\text{Nd recovery (\%)} = 69.51 + 15.26A + 0.55B \quad (5)$$

where A and B denote the coded values of hydrochloric acid concentration and leaching temperature, respectively. The intercept (69.51) represents the predicted Nd recovery at the center point of the experimental design. The coefficient associated with hydrochloric acid concentration (+15.26) indicates that each unit increase in the coded acid concentration produces an average increase of approximately 15.26% in neodymium recovery, confirming that acid concentration is the dominant parameter governing the leaching process. In comparison, the coefficient corresponding to temperature (+0.55) is considerably smaller, indicating only a slight positive influence on Nd extraction. Consistent with the ANOVA results ($p = 0.8226$), this contribution is not statistically significant, demonstrating that temperature plays only a minor role in controlling neodymium recovery within the investigated operating range.

Table 8. Analysis of variance (ANOVA) for the developed regression model of neodymium (Nd) recovery.

ANOVA component	DOF	Sum of squares (SS)	Mean square (MS)	F-statistic	Probability (p)	Statistical interpretation
Regression model	2	2468.88	1234.44	6.14	0.0057	Significant
Hydrochloric acid concentration (A)	1	2458.61	2458.61	12.23	0.0014	Significant
Leaching temperature (B)	1	10.27	10.27	0.0511	0.8226	Not significant
Residual error	31	6230.38	200.98	—	—	—
Total corrected variation	33	8699.26	—	—	—	—

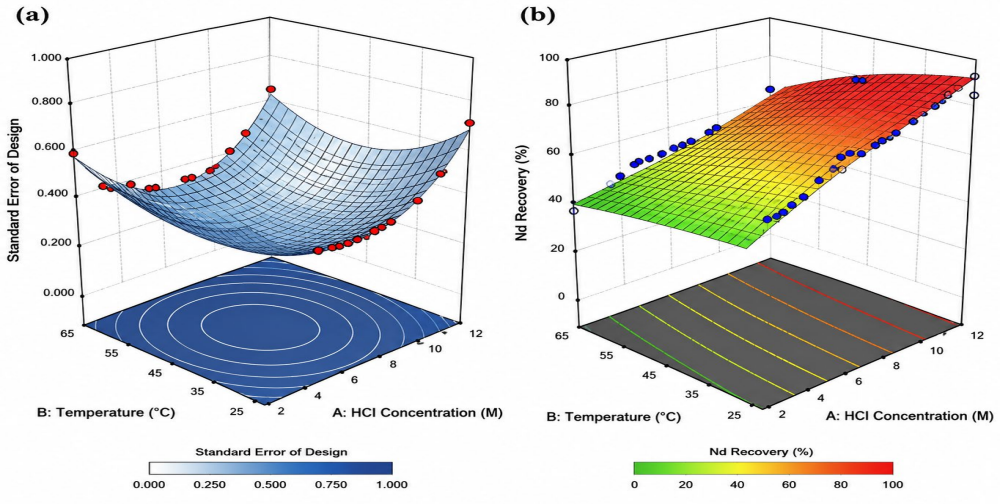

Fig. 5. a) Distribution of the standard error over the design surface and b) three-dimensional response surface representing Nd recovery.

Fig. 5 presents two three-dimensional surface plots that characterize the statistical performance of the developed model and the behavior of Nd leaching in relation to acid concentration (M) and temperature (T). Panel a displays the spatial distribution of the model's standard error throughout the experimental design domain, whereas panel b depicts the predicted response surface describing Nd recovery (%). Collectively, these figures provide a comprehensive assessment of both the statistical robustness of the experimental design and the influence of the selected operating variables on leaching efficiency. The standard error surface shown in Fig. 5a demonstrates how prediction uncertainty varies with acid concentration and temperature. The lowest standard error values are observed near the center of the design space, corresponding approximately to an acid concentration of 7–9 M and a temperature range of 40–50 °C. This region represents the highest predictive accuracy of the response surface model, indicating that model estimates within these operating conditions are statistically more reliable. As the experimental conditions approach the boundaries of the investigated domain, including very low or very high acid concentrations and temperatures, the prediction error increases slightly. Such behavior is characteristic of response surface methodology because fewer design points exist near the experimental limits, reducing model precision and increasing uncertainty. The accompanying contour map further confirms this pattern, with closely spaced contour lines concentrated around the central region, reflecting the highest design resolution. Overall, these observations demonstrate the adequacy of the selected experimental domain and verify that the statistical model effectively captures the behavior of the leaching system. Fig. 5b illustrates the predicted variation in neodymium recovery as a combined function of acid concentration and temperature. A pronounced enhancement in Nd recovery is observed as the acid concentration increases from approximately 2 M to 13.6 M, indicating that acid strength is the principal parameter governing the dissolution process. Higher proton availability promotes the breakdown of neodymium-containing mineral phases, thereby increasing the extent of metal extraction. The response surface exhibits a steep slope along the acid concentration axis, emphasizing its dominant influence on leaching performance. In comparison, the temperature axis displays a much gentler gradient, indicating that temperature has a relatively limited effect within the investigated interval of 25–65 °C. Although elevated temperatures produce a slight improvement in recovery, their contribution remains considerably smaller than that of acid concentration. This behavior is consistent with the established principles of acid leaching, where acid concentration primarily determines the chemical driving force for mineral dissolution, whereas temperature mainly accelerates reaction kinetics. Another important feature of the response surface is the gradual formation of a plateau at high acid concentrations combined with moderate to elevated temperatures. Under these conditions, Nd recovery approaches or exceeds 90%, suggesting that the extraction process is approaching its practical maximum. This leveling of the response indicates diminishing incremental benefits from further increases in acid concentration once a critical threshold has been reached. From an engineering perspective, this behavior is particularly significant because it suggests that excessive acid consumption may not produce proportional improvements in recovery. Consequently, an appropriate balance between acid dosage and extraction efficiency can improve process economics while simultaneously reducing environmental impacts associated with reagent consumption. Taken together, the two response surface plots provide a comprehensive understanding of both model quality and process performance. The standard error distribution

Table 9. Regression coefficients and statistical parameters of the developed model for neodymium (Nd) recovery.

Predictor	Regression coefficient	SE	95% CI	df	VIF
Intercept	69.51	2.51	64.40 to 74.62	1	—
Acid concentration (A)	15.26	4.36	6.36 to 24.16	1	1.000
Temperature (B)	0.5497	2.43	-4.41 to 5.51	1	1.000

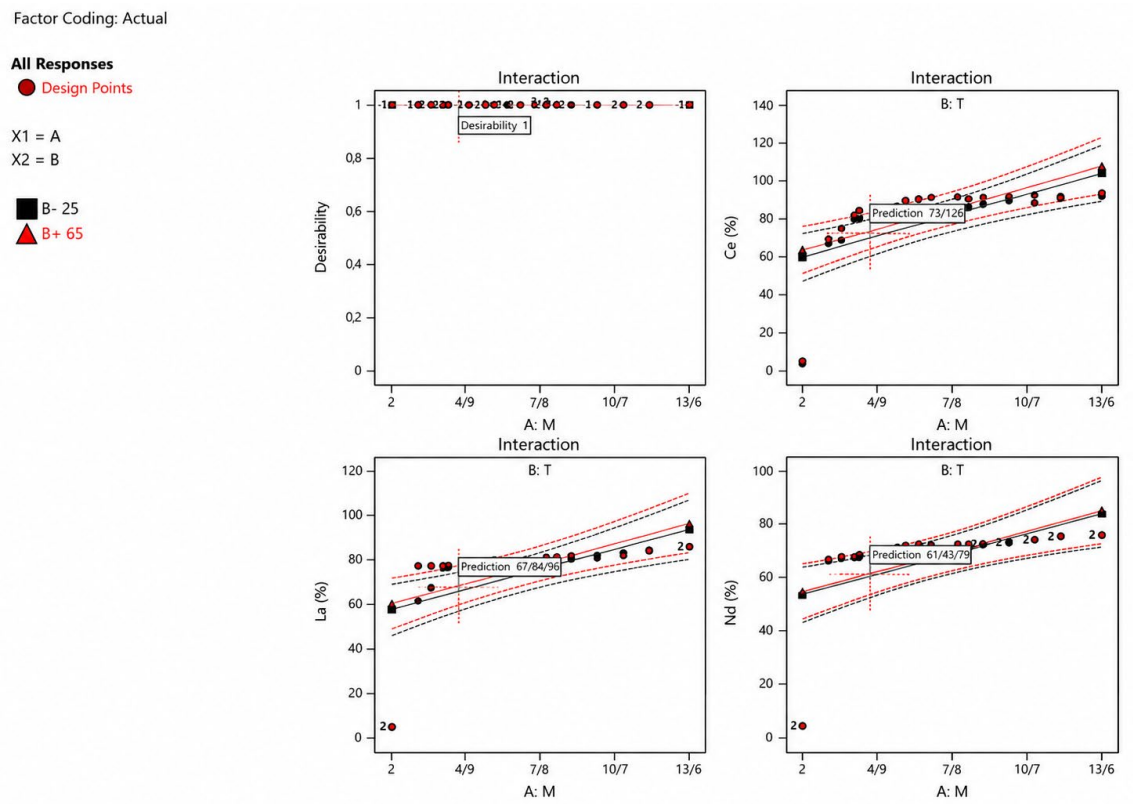

Fig. 6. Interaction plots and desirability analysis for the recovery of cerium (Ce), lanthanum (La), and neodymium (Nd).

demonstrates that the developed statistical model exhibits its greatest predictive reliability within the central region of the experimental design, while the response surface clearly identifies acid concentration as the primary factor controlling neodymium recovery. These findings indicate that high extraction efficiencies can be achieved using relatively high acid concentrations in combination with moderately elevated temperatures, providing practical guidance for optimizing rare earth leaching processes while maintaining both operational efficiency and environmental sustainability.

Fig. 6 illustrates the interaction plots generated from the fitted response surface model, showing the combined influence of hydrochloric acid concentration (A) and leaching temperature (B) on the recovery of Ce, La, and Nd, together with the corresponding desirability profile. For cerium, the response curve exhibits a pronounced positive trend with increasing hydrochloric acid concentration, confirming that acid molarity is the primary factor governing Ce dissolution. At both investigated temperatures (25 and 65 °C), cerium recovery increased steadily as the HCl concentration increased from 2.0 to 13.6 M, with the highest recovery approaching 94.2% under the most concentrated acid conditions. The nearly parallel response lines obtained at the two temperature levels indicate that the interaction between acid concentration and temperature is relatively weak, suggesting that the contribution of temperature to cerium extraction is considerably smaller than that of acid concentration. This observation is in excellent agreement with the ANOVA results, where hydrochloric acid concentration was identified as a statistically significant factor ($F = 18.13$, $p = 0.0002$), whereas the effect of temperature was found to be insignificant ($F = 0.437$, $p = 0.5134$). The desirability profile further demonstrates that the optimization objective was successfully achieved throughout the investigated design space, with desirability values approaching unity over a broad range of operating conditions. The highest desirability coincides with the region corresponding to elevated acid concentration and higher temperature, indicating that these operating conditions maximize cerium recovery while satisfying the optimization criteria imposed by the response surface model. The narrow prediction intervals surrounding the fitted regression lines and the close agreement between the experimental observations and model predictions further confirm the adequacy of the developed regression model. Overall, the interaction analysis demonstrates that increasing hydrochloric acid concentration is the dominant driving force for cerium leaching, whereas temperature provides only a modest enhancement within the investigated range of 25–65 °C. Consequently, optimization of the leaching process should primarily focus on controlling acid concentration, while temperature may be adjusted as a secondary operational parameter to maximize cerium recovery without introducing unnecessary energy consumption.

3.3. SEM characterization of leaching residues

SEM examination of the residues obtained after hydrochloric acid leaching of the apatite-bearing iron ore clearly revealed significant morphological differences among the samples treated with 2 M, 4 M, and 6.5 M HCl. These variations directly reflect the extent of dissolution reactions and the degree of decomposition of acid-sensitive mineral phases under different leaching conditions.

For the sample leached with 2 M HCl (Fig. 7a–c), the residue mainly consists of dispersed and isolated particles deposited on the filter

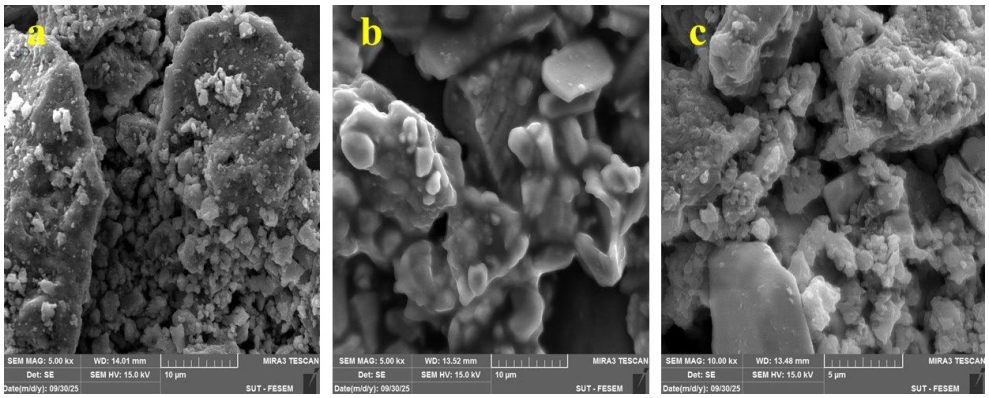

Fig. 7. SEM micrographs of the solid residue collected by filtration after leaching with 2 M HCl.

surface. Most particles exhibit sizes ranging from approximately 5 to 10 µm, and several grains retain their original crystalline morphology. Well-defined flat faces, sharp edges, and angular geometries are still evident, indicating that the crystalline framework remains relatively stable under these leaching conditions. The particle surfaces appear predominantly smooth, with only slight evidence of surface etching or localized dissolution. These observations indicate that the acid concentration is insufficient to induce extensive structural degradation of the apatite lattice, and the dissolution process is therefore largely confined to the outer particle surfaces. The limited morphological alteration can be attributed to the relatively low proton activity at 2 M HCl, which restricts the proton-assisted cleavage of Ca–O and P–O bonds within the apatite crystal structure. Since the dissolution of apatite proceeds through the progressive protonation of phosphate groups followed by the release of Ca^{2+}, phosphate species, and structurally incorporated REE^{3+} ions, an insufficient concentration of H^+ slows the overall dissolution kinetics and prevents continuous lattice decomposition. Under these conditions, dissolution preferentially occurs at high-energy surface sites, including crystal defects, dislocations, microcracks, and grain boundaries, where the activation energy for bond rupture is lower than that of the well-ordered crystal planes. As a result, only localized surface attacks are observed, while the bulk crystalline framework remains largely intact. Another important factor contributing to the limited dissolution is the relatively low concentration gradient between the solid surface and the bulk leaching solution. A lower proton concentration reduces the driving force for interfacial reactions and decreases the frequency of effective collisions between hydrogen ions and reactive surface sites. Consequently, the dissolution rate becomes predominantly controlled by surface reaction kinetics rather than by diffusion, leading to only minor surface roughening and shallow etch pits instead of extensive particle fragmentation or pore development. Furthermore, the preservation of well-defined crystal faces suggests that crystallographic anisotropy plays an important role during the early stages of leaching. Crystal planes with lower surface energy and higher atomic packing density exhibit greater resistance to proton attack, whereas dissolution preferentially initiates along structurally defective regions. This selective dissolution mechanism explains why the overall particle geometry remains nearly unchanged despite the occurrence of limited surface corrosion. The absence of widespread cracking or structural collapse also indicates that acid penetration into the particle interior is minimal at this concentration, preventing the propagation of dissolution fronts toward the particle core. From a chemical perspective, the persistence of phosphorus- and calcium-rich particles in the residue is therefore expected, providing further evidence that a substantial fraction of the apatite matrix remains undissolved. Because Ce, La, and Nd predominantly substitute for Ca within the apatite lattice, their dissolution is intrinsically linked to the decomposition of the host mineral. Consequently, the incomplete breakdown of the apatite structure directly limits the liberation of these rare earth elements into the leach solution, resulting in relatively low extraction efficiencies. The strong agreement between the preserved crystalline morphology observed in the SEM images and the comparatively poor REE recoveries demonstrates that the structural integrity of the apatite grains is closely correlated with leaching performance. Therefore, the SEM observations provide direct microstructural evidence that 2 M HCl does not supply sufficient chemical driving force to achieve effective apatite decomposition, confirming that acid concentration is the dominant parameter controlling both mineral dissolution and REE release.

As shown in Fig. 8a–c, increasing the HCl concentration to 4 M results in a pronounced modification of the residue morphology compared with that observed after leaching in 2 M HCl. The SEM micrographs clearly reveal the onset of significant changes in particle geometry, accompanied by the gradual deterioration of the original crystalline framework, indicating that mineral dissolution has progressed beyond the initial surface-etching stage. The formerly well-defined crystal faces become increasingly irregular, while particle edges lose their sharpness and exhibit localized rounding, suggesting that dissolution is no longer restricted to isolated surface defects but has propagated across larger crystallographic domains. The enhanced structural degradation can be attributed to the higher proton activity in the leaching solution, which substantially accelerates the proton-assisted disruption of the apatite lattice. At 4 M HCl, the increased availability of hydrogen ions promotes more extensive protonation of phosphate tetrahedra, thereby weakening the Ca–O and P–O bonds that maintain the structural integrity of the mineral. As these bonds are progressively broken, calcium ions together with structurally substituted rare earth elements (Ce^{3+}, La^{3+}, and Nd^{3+}) are released into the solution at a significantly higher rate than observed at lower acid concentrations. Consequently, the dissolution front advances deeper into the particles rather than remaining confined to the external surface, leading to progressive collapse of the crystalline architecture. Unlike the residue obtained at 2 M HCl, where dissolution is largely limited to high-energy sites such as crystal defects and grain boundaries, the higher

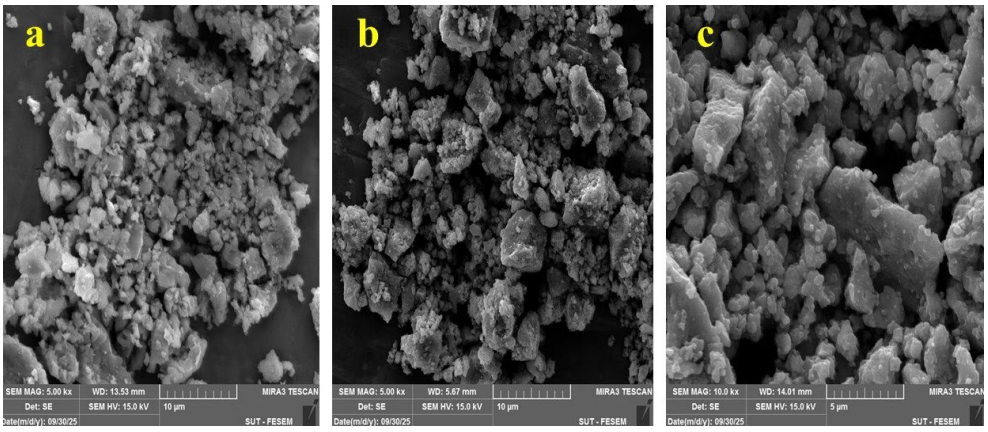

Fig. 8. SEM micrographs of the solid residue collected by filtration after leaching with 4 M HCl.

acid concentration provides sufficient chemical driving force to activate dissolution over relatively stable crystallographic planes. This transition suggests that the dissolution mechanism changes from localized surface attack to a more homogeneous and continuous dissolution process affecting the entire particle. As a result, the original faceted morphology becomes increasingly distorted, reflecting the progressive recession of crystallographic surfaces and the loss of long-range structural order. The observed morphological evolution also indicates a significant increase in the density of reactive surface sites generated during leaching. As dissolution proceeds, newly exposed surfaces continuously replace those that have already reacted, effectively increasing the available surface area for further acid attack. This positive feedback mechanism accelerates the overall dissolution kinetics, since the formation of fresh surfaces facilitates additional proton adsorption and enhances mineral–solution interfacial reactions. Simultaneously, the development of microcracks and shallow surface depressions improves acid penetration into the particle interior, reducing diffusion limitations and allowing the leaching solution to access previously unreacted regions of the apatite grains. From a crystallographic standpoint, the progressive disappearance of flat crystal faces suggests that dissolution becomes increasingly isotropic with increasing acid concentration. In the early stages of leaching, crystallographic anisotropy governs the preferential dissolution of high-energy planes, whereas at 4 M HCl the chemical potential of the solution becomes sufficiently high to overcome differences in surface energy between crystallographic orientations. Consequently, dissolution proceeds simultaneously along multiple crystal planes, producing a more irregular particle morphology and reducing the geometric stability of the residual grains. The initiation of pore formation observed in several particles further supports this interpretation. These pores most likely originate from the preferential dissolution of chemically heterogeneous regions enriched in calcium and phosphate, creating localized voids that gradually coalesce as leaching progresses. Such pore development not only reflects mineral decomposition but also substantially enhances internal mass transport by increasing solution accessibility to the particle core. This phenomenon is particularly important because the rare earth elements are incorporated within the apatite lattice rather than existing as discrete mineral phases. Therefore, the formation of interconnected pores facilitates the exposure of previously inaccessible REE-bearing regions, promoting their subsequent dissolution. From a chemical perspective, the reduction in the abundance of phosphorus- and calcium-rich particles compared with the 2 M residue provides strong evidence that apatite decomposition becomes considerably more extensive at 4 M HCl. Since the dissolution of Ce, La, and Nd is directly coupled with the breakdown of the calcium phosphate framework, the more pronounced structural degradation observed in the SEM micrographs is consistent with the higher REE extraction efficiencies obtained experimentally. The close agreement between the microstructural observations and the leaching results confirms that increasing hydrochloric acid concentration not only accelerates the dissolution kinetics but also fundamentally alters the dissolution mechanism by promoting bulk lattice degradation rather than localized surface corrosion. Accordingly, the SEM analysis provides direct mechanistic evidence that the transition from 2 M to 4 M HCl represents a critical stage in the evolution of apatite dissolution, where both structural collapse and REE liberation become significantly more pronounced.

In contrast, the residue obtained after leaching with 6.5 M HCl (Fig. 9a–c) exhibits substantially more severe structural degradation than the residues produced at 2 M and 4 M HCl. Rather than consisting of discrete crystalline particles, the solid residue appears as highly porous agglomerates with irregular, fragmented morphologies. The original crystalline facets have almost completely disappeared, and the particle surfaces are characterized by extensive corrosion, deep dissolution pits, irregular fractures, collapsed crystal boundaries, and an interconnected network of fine pores. Such profound morphological transformation indicates that the original apatite structure has undergone extensive destruction as a consequence of the highly aggressive acidic environment. The pronounced structural collapse observed at 6.5 M HCl reflects a fundamental change in the dissolution behavior of apatite. At this acid concentration, the activity of hydrogen ions is sufficiently high to sustain continuous proton-assisted dissolution over the entire particle surface, eliminating the localized dissolution behavior observed at lower acid concentrations. The rapid protonation of phosphate groups continuously weakens the Ca–O and P–O bonds that stabilize the apatite lattice, allowing the dissolution front to propagate rapidly from the external surface toward the particle interior. Consequently, mineral decomposition is no longer limited by the availability of reactive surface sites but instead proceeds throughout the entire crystal volume, resulting in extensive lattice destabilization and eventual structural collapse. The almost complete disappearance of

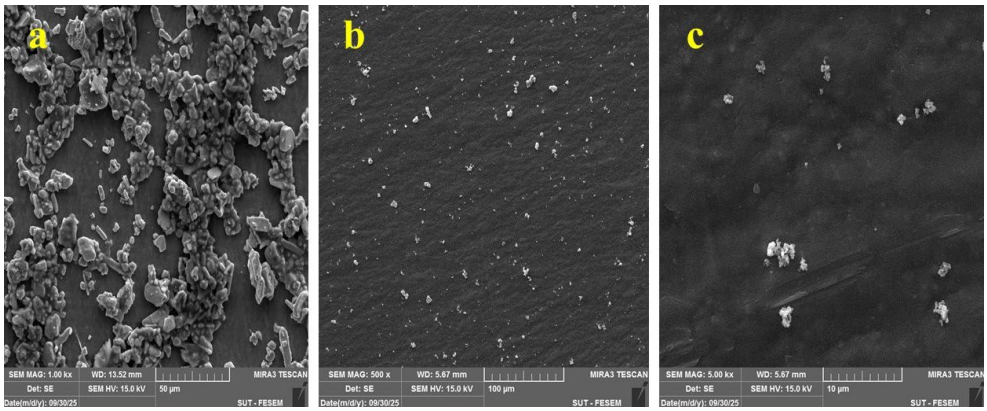

Fig. 9. SEM micrographs of the solid residue collected by filtration after leaching with 6.5 M HCl.

well-defined crystallographic faces provides strong evidence that the long-range crystallographic order of apatite has been largely destroyed. Unlike the selective dissolution observed at lower acid concentrations, where crystallographic orientation influences the dissolution rate, the highly acidic environment significantly reduces the anisotropic nature of mineral dissolution. Under these conditions, proton attack becomes sufficiently energetic to overcome differences in surface energy among crystallographic planes, leading to nearly uniform dissolution across the crystal. As a result, the original faceted morphology is replaced by irregular particle fragments with no recognizable crystallographic features, indicating that the residual material has lost most of its original structural integrity. Another remarkable feature evident in the SEM micrographs is the extensive development of interconnected pores and microfractures throughout the residue. The formation of these pores is attributed to the preferential dissolution of calcium phosphate domains within the apatite matrix, which progressively generates internal voids that eventually merge into a continuous porous network. Simultaneously, the release of structurally incorporated Ca^{2+} ions creates localized vacancies within the crystal lattice, further weakening the mineral framework and promoting crack propagation. The combined effect of pore coalescence and fracture development dramatically increases the internal surface area exposed to the leaching solution, thereby facilitating deeper penetration of hydrochloric acid into previously inaccessible regions of the particles. This continuous generation of fresh reactive surfaces establishes a self-accelerating dissolution process in which newly exposed mineral surfaces become immediately available for further proton attack, significantly enhancing the overall dissolution kinetics. From a mass-transfer perspective, the highly porous microstructure substantially reduces diffusion resistance within the particles. At lower acid concentrations, dissolution is primarily governed by surface reaction kinetics because acid penetration into the particle interior is limited. However, the interconnected pore network formed at 6.5 M HCl provides efficient transport pathways for both hydrogen ions entering the particle and dissolved reaction products leaving the solid matrix. This enhanced internal diffusion minimizes concentration gradients between the particle surface and core, allowing dissolution reactions to proceed more uniformly throughout the entire particle volume. Consequently, the overall leaching process transitions from a surface-controlled mechanism toward one in which rapid interfacial reactions and efficient mass transport occur simultaneously, greatly improving extraction efficiency. The observed structural degradation also provides direct evidence for the enhanced liberation of rare earth elements. Because cerium, lanthanum, and neodymium are predominantly incorporated into the apatite lattice through isomorphic substitution for calcium, their release into the leach solution is intrinsically dependent on the destruction of the host crystal structure. Therefore, the extensive lattice collapse observed in the SEM images strongly supports the experimentally measured increase in REE recoveries. Rather than being released solely from the particle surface, the rare earth elements become progressively accessible as dissolution penetrates deeper into the crystal, resulting in significantly higher extraction efficiencies. This close correspondence between microstructural evolution and leaching performance demonstrates that the degree of crystal destruction is an effective indicator of REE liberation. Another consequence of the extensive apatite dissolution is the progressive enrichment of relatively acid-resistant mineral phases within the solid residue. As calcium phosphate minerals are preferentially dissolved and transferred into the solution, minerals exhibiting greater chemical stability under strongly acidic conditions, particularly silica-rich phases and iron oxides, become increasingly concentrated in the remaining solid. This relative enrichment should not be interpreted as the formation of new mineral phases but rather as the selective removal of the more reactive apatite component. Such selective dissolution is consistent with the marked reduction in phosphorus- and calcium-bearing particles observed in the SEM images and further confirms that the majority of the apatite matrix has been removed during leaching. It is also noteworthy that residues produced at this acid concentration may retain detectable amounts of chlorine if washing is incomplete. Under highly acidic conditions, concentrated chloride solutions can remain trapped within the interconnected pore network or adsorbed onto the large specific surface area generated during dissolution. Consequently, residual chloride detected by elemental analysis is more likely to originate from physically retained leach solution or adsorbed chloride species than from the formation of stable chloride-bearing mineral phases. Overall, the SEM observations clearly demonstrate that increasing the hydrochloric acid concentration to 6.5 M fundamentally changes the dissolution mechanism of apatite. The transition from localized surface etching observed at 2 M, through progressive lattice degradation at 4 M, to extensive structural collapse and highly porous

residual frameworks at 6.5 M provides compelling microstructural evidence for the continuous enhancement of apatite decomposition. These observations are fully consistent with statistical optimization results, which identify acid concentration as the dominant parameter controlling REE extraction. The excellent agreement between the SEM characterization and the leaching data confirms that the superior recoveries of Ce, La, and Nd obtained under these conditions originate directly from the nearly complete destruction of the apatite crystal structure, thereby establishing a clear mechanistic relationship between acid-induced microstructural evolution and rare earth element liberation.

4. Conclusions

This study systematically investigated the hydrochloric acid leaching behavior of cerium (Ce), lanthanum (La), and neodymium (Nd) from an apatite concentrate obtained from iron ore processing waste by integrating statistical analysis with microstructural characterization. Response Surface Methodology (RSM) combined with central composite design (CCD) was employed to evaluate the influence of hydrochloric acid concentration and leaching temperature on rare earth element recovery, while the solid-to-liquid ratio (1:9) and leaching time (60 min) were maintained constant throughout the experimental program. The statistical analysis demonstrated that hydrochloric acid concentration was the dominant operational factor affecting the dissolution of all investigated rare earth elements, whereas temperature exhibited a comparatively smaller influence within the studied range. Under the selected fixed operating conditions of a solid-to-liquid ratio of 1:9 and a leaching time of 60 min, the highest recoveries were achieved at 37 wt% HCl (13.6 M) and 65 °C, yielding extraction efficiencies of 94.19% for Ce, 86.33% for La, and 76.34% for Nd. Although the developed linear regression models explained a moderate proportion of the experimental variability, they successfully described the principal influence of hydrochloric acid concentration on rare earth element recovery within the investigated design space and provided a practical basis for process evaluation. SEM observations further supported the statistical findings by revealing progressive surface corrosion, pore development, particle fragmentation, and gradual destruction of the apatite matrix as acid concentration increased. These microstructural changes were closely associated with enhanced mineral decomposition and improved liberation of rare earth elements, providing direct experimental evidence for the dominant role of hydrochloric acid concentration in the leaching mechanism. From an engineering perspective, although the maximum recoveries were obtained using 37 wt% HCl, only marginal improvements were observed beyond approximately 6.5 M HCl, indicating that intermediate acid concentrations may provide a more favorable compromise between reagent consumption, operating costs, and metal recovery. Therefore, depending on economic considerations and process objectives, hydrochloric acid concentrations around 6.5 M may represent a practical operating alternative for large-scale implementation. Overall, the present work demonstrates the technical feasibility of recovering valuable rare earth elements from apatite-rich iron ore processing residues through hydrochloric acid leaching and provides useful experimental and microstructural information for the future development and optimization of sustainable hydrometallurgical recovery processes.

CRediT authorship contribution statement

Erfan Mohammadzadeh: Methodology, Formal Analysis, Data curation, Investigation, Writing – original draft.
Sayed Khatiboleslam Sadrnezhaad: Writing – review & editing, Supervision.
Hossein Yoozbashizadeh: Writing – review & editing, Supervision.
Mahdi Maarefvand: Data curation.

Data availability

The data supporting the findings of this study are available from the corresponding author upon reasonable request. No publicly accessible repository was used for this study.

Declaration of competing interest

The authors declare that they have no known competing financial interests or personal relationships that could have appeared to influence the work reported in this paper.

Funding and acknowledgment

This research received no specific grant from funding agencies in the public, commercial, or not-for-profit sectors.

Declaration of Ai and Ai-assisted technologies in the writing process

During the preparation of this manuscript, the authors used artificial intelligence (AI)-assisted tools, including large language models (LLMs), to improve the linguistic quality of the manuscript, assist in drafting and refining selected scientific descriptions, support the interpretation of certain experimental results, and perform minor graphical modifications to several figures for improved clarity and presentation. AI tools were not used to generate experimental data, perform laboratory experiments, or make independent scientific decisions. All data analyses, scientific interpretations, conclusions, and final editorial decisions were carefully verified and approved by the authors, who take full responsibility for the content and integrity of the manuscript.

References

[1] A. Ford, D. Huston, J. Cloutier, M. Doublier, A. Schofield, et al., A national-scale mineral potential assessment for carbonatite-related rare earth element mineral systems in Australia, Ore Geol. Rev. 161 (2023) 105658. https://doi.org/10.1016/j.oregeorev.2023.105658.
[2] Y. Ghorbani, I.M.S.K. Ilankoon, N. Dushyantha, G.T. Nwaila, Rare earth permanent magnets for the green energy transition: Bottlenecks, current developments and cleaner production solutions, Resour. Conserv. Recycl. 212 (2025) 107966. https://doi.org/10.1016/j.resconrec.2024.107966.
[3] H. Diao, H. Yang, T. Tan, G. Ren, M. You, et al., Navigating the rare earth elements landscape: Challenges, innovations, and sustainability, Miner. Eng. 216 (2024) 108889. https://doi.org/10.1016/j.mineng.2024.108889.
[4] D.A. Tamayo-Soriano, M.D.J. Soria-Aguilar, N.G. Picazo-Rodríguez, A. Martínez-Luévanos, F.R. Carrillo-Pedroza, et al., Acid leaching

of La and Ce from ferrocarbonatite-related REE ores, Minerals. 14 (2024) 504. https://doi.org/10.3390/min14050504.
[5] D. Kołodyńska, D. Fila, B. Gajda, J. Gęga, Z. Hubicki, Rare earth elements separation methods yesterday and today, in: Applications of Ion Exchange Materials in the Environment, Springer International Publishing, Cham. (2019) 161–185. https://doi.org/10.1007/978-3-030-10430-6_8.
[6] L.M. Suli, W.H.W. Ibrahim, B.A. Aziz, M.R. Deraman, N.A. Ismail, A review of rare earth mineral processing technology, Chem. Eng. Res. Bull. 19 (2017) 20–35. https://doi.org/10.3329/cerb.v19i0.33773.
[7] W.F. Holmes-Hewett, J.D. Miller, H.G. Ahmad, S. Granville, B.J. Ruck, Rare-earth nitrides: fundamental advances and applications in cryogenic electronics, J. Phys. D Appl. Phys. 58 (2025) 343001. https://doi.org/10.1088/1361-6463/adf1b2.
[8] S. Pramanik, S. Kaur, I. Popovs, A.S. Ivanov, S. Jansone-Popova, Emerging rare earth element separation technologies, Eur. J. Inorg. Chem. 27 (2024) e202400064. https://doi.org/10.1002/ejic.202400064.
[9] B. Zhou, Z. Li, C. Chen, Global potential of rare earth resources and rare earth demand from clean technologies, Minerals. 7 (2017) 203. https://doi.org/10.3390/min7110203.
[10] O. Artiushenko, R.F. da Silva, V. Zaitsev, Recent advances in functional materials for rare earth recovery: A review, Sustain. Mater. Technol. 37 (2023) e00681. https://doi.org/10.1016/j.susmat.2023.e00681.
[11] G. Azimi, Technological advancements in rare earth elements recovery from ionic clays: a comprehensive review, Hydrometallurgy. 231 (2025) 106414. https://doi.org/10.1016/j.hydromet.2024.106414.
[12] D. Alferova, Rare earth metals recovery from apatite processing products using liquid-liquid extraction method, Master's Thesis. (2022). https://doi.org/10.34901/mul.pub.2023.94.
[13] M. Peiravi, F. Dehghani, L. Ackah, A. Baharlouei, J. Godbold, et al., A review of rare-earth elements extraction with emphasis on non-conventional sources: Coal and coal byproducts, iron ore tailings, apatite, and phosphate byproducts, Min. Metall. Explor. 38 (2021) 1–26. https://doi.org/10.1007/s42461-020-00307-5.
[14] E. Jorjani, A.H. Bagherieh, S.C. Chelgani, Rare earth elements leaching from Chadormalu apatite concentrate: Laboratory studies and regression predictions, Korean J. Chem. Eng. 28 (2011) 557–562. https://doi.org/10.1007/s11814-010-0383-4.
[15] F. Ahani, M. Osali, H. Khodaei, S. Karimi, J. Moghaddam, Efficient recovery of rare earth elements from apatite concentrate via pre-leaching, pressure leaching, and precipitation: Process evaluation, Hydrometallurgy. 232 (2025) 106429. https://doi.org/10.1016/j.hydromet.2024.106429.
[16] A. Ferdowsi, H. Yoozbashizadeh, Process optimization and kinetics for leaching of cerium, lanthanum and neodymium elements from iron ore waste's apatite by nitric acid, Trans. Nonferrous Met. Soc. China. 27 (2017) 420–428. https://doi.org/10.1016/S1003-6326(17)60048-7.
[17] K. Binnemans, P.T. Jones, B. Blanpain, T. Van Gerven, Y. Yang, et al., Recycling of rare earths: a critical review, J. Clean. Prod. 51 (2013) 1–22. https://doi.org/10.1016/j.jclepro.2012.12.037.
[18] P. Josso, S. Roberts, D.A. Teagle, O. Pourret, R. Herrington, C.P. de Leon Albarran, Extraction and separation of rare earth elements from hydrothermal metalliferous sediments, Miner. Eng. 118 (2018) 106–121. https://doi.org/10.1016/j.mineng.2017.12.014.
[19] R. Kim, H. Cho, K.N. Han, K. Kim, M. Mun, Optimization of acid leaching of rare-earth elements from Mongolian apatite-based ore, Minerals. 6 (2016) 63. https://doi.org/10.3390/min6030063.
[20] K. Stone, A.M.T.S. Bandara, G. Senanayake, S. Jayasekera, Processing of rare earth phosphate concentrates: A comparative study of pre-leaching with perchloric, hydrochloric, nitric and phosphoric acids and deportment of minor/major elements, Hydrometallurgy. 163 (2016) 137–147. https://doi.org/10.1016/j.hydromet.2016.03.014.
[21] A. Battsengel, A. Batnasan, A. Narankhuu, K. Haga, Y. Watanabe, A. Shibayama, Recovery of light and heavy rare earth elements from apatite ore using sulphuric acid leaching, solvent extraction and precipitation, Hydrometallurgy. 179 (2018) 100–109. https://doi.org/10.1016/j.hydromet.2018.05.024.
[22] E.V. Smirnova, I.N. Fedorova, G.P. Sandimirova, L.L. Petrov, N.G. Balbekina, V.I. Lozhkin, Determination of rare earth elements in black shales by inductively coupled plasma mass spectrometry, Spectrochim. Acta B. At. Spectrosc. 58 (2003) 329–340. https://doi.org/10.1016/S0584-8547(02)00152-0.
[23] G. Pandey, S. Mukhopadhyay, A.U. Renjith, J.M. Joshi, K.T. Shenoy, Recovery of Hf and Zr from slurry waste of zirconium purification plant using solvent extraction, Hydrometallurgy. 163 (2016) 61–68. https://doi.org/10.1016/j.hydromet.2016.03.005.
[24] X. Yang, R.Q. Honaker, Leaching kinetics of rare earth elements from fire clay seam coal, Minerals. 10 (2020) 491. https://doi.org/10.3390/min10060491.
[25] X. Li, W. Li, Y. Gao, G. Tian, Effect of mechanical activation on the leaching process of rare earth metal yttrium in deep eutectic solvents, Appl. Sci. 12 (2022) 8253. https://doi.org/10.3390/app12168253.
[26] S. Diallo, L.-H. Tran, D. Larivière, J.-F. Blais, Selective leaching of rare earths, base metals and precious metals from used smartphones, Environ. Technol. 46 (2025) 2149–2164. https://doi.org/10.1080/09593330.2024.2423906.
[27] S.F. Lütke, M.L. Oliveira, S.R. Waechter, L.F. Silva, T.R. Cadaval Jr., et al., Leaching of rare earth elements from phosphogypsum, Chemosphere. 301 (2022) 134661. https://doi.org/10.1016/j.chemosphere.2022.134661.
[28] A.R. Ray, B.C. Tripathy, S. Mishra, Leaching of rare earth elements from phosphogypsum via citric acid medium: optimization through central composite design and kinetics studies, Environ. Sci. Pollut. Res. Int. 32 (2025) 4076–4089. https://doi.org/10.1007/s11356-025-35908-4.
[29] J.-L. Mukaba, C.P. Eze, O. Pereao, L.F. Petrik, Rare earths' recovery from phosphogypsum: An overview on direct and indirect leaching techniques, Minerals. 11 (2021) 1051. https://doi.org/10.3390/min11101051.
[30] N. Hurtado-Alonso, J. Manso-Morato, V. Revilla-Cuesta, M. Skaf, V. Ortega-Lopez, Optimization of cementitious mixes through response surface method: a systematic review, Arch. Civ. Mech. Eng. 25 (2024) 54. https://doi.org/10.1007/s43452-024-01112-3.
[31] S.A. Khan, Application of central composite design (CCD)-response surface methodology (RSM) for optimization of heat transfer in dusty nanofluid flow with velocity slip, Numer. Heat Transf. A: Appl. 87 (2026) 2372044. https://doi.org/10.1080/10407782.2024.2372044.
[32] L. Lovia, Y. Yusnita, A. Dwinata, Linear regression to analyze temperature and air humidity on rainfall: a case study at Padang Panjang geophysics station (2020–2023), Rangkiang Math. J. 3 (2024) 46–53. https://doi.org/10.24036/rmj.v3i2.60.